



This is a repository copy of *Two-dimensional angular parameter estimation for noncircular incoherently distributed sources based on an L-shaped array*.

White Rose Research Online URL for this paper:
<https://eprints.whiterose.ac.uk/162924/>

Version: Accepted Version

Article:

Chen, H., Liu, Y., Wang, Q. et al. (2 more authors) (2020) Two-dimensional angular parameter estimation for noncircular incoherently distributed sources based on an L-shaped array. *IEEE Sensors Journal*, 20 (22). pp. 13704-13715. ISSN 1530-437X

<https://doi.org/10.1109/jsen.2020.3006431>

© 2020 IEEE. Personal use of this material is permitted. Permission from IEEE must be obtained for all other users, including reprinting/ republishing this material for advertising or promotional purposes, creating new collective works for resale or redistribution to servers or lists, or reuse of any copyrighted components of this work in other works. Reproduced in accordance with the publisher's self-archiving policy.

Reuse

Items deposited in White Rose Research Online are protected by copyright, with all rights reserved unless indicated otherwise. They may be downloaded and/or printed for private study, or other acts as permitted by national copyright laws. The publisher or other rights holders may allow further reproduction and re-use of the full text version. This is indicated by the licence information on the White Rose Research Online record for the item.

Takedown

If you consider content in White Rose Research Online to be in breach of UK law, please notify us by emailing eprints@whiterose.ac.uk including the URL of the record and the reason for the withdrawal request.



eprints@whiterose.ac.uk
<https://eprints.whiterose.ac.uk/>

Two-dimensional angular parameter estimation for noncircular incoherently distributed sources based on an L-shaped array

Hua Chen, *Member, IEEE*, Yonghong Liu, Qing Wang, *Member, IEEE*, Wei Liu, *Senior Member, IEEE*, and Gang Wang, *Senior Member, IEEE*

Abstract—In this paper, a two-stage reduced-rank estimator is proposed for two-dimensional (2D) direction estimation of incoherently distributed (ID) noncircular sources, including their center directions of arrival (DOAs) and angular spreads, based on an L-shaped array. Firstly, based on the first-order Taylor series approximation, a noncircularity-based extended generalized array manifold (GAM) model is established. Then, the 2D center DOAs of incident ID signals are obtained separately with the noncircularity-based generalized shift-invariance property of the array manifold and the reduced-rank principle. The pairing of the two center DOAs is completed by searching for the minimum value of a cost function. Secondly, the 2D angular spreads can be obtained in closed-form solution from the central moments of the angular distribution. The proposed estimator achieves higher accuracy in angle estimation that manages more sources and shows promising results in the general scenario, where different sources possess different angular distributions. Furthermore, the approximate noncircular stochastic Cramer-Rao bound (CRB) of the concerned problem is derived as a benchmark. Numerical analysis proves that the proposed algorithm achieves better estimation performance in both 2D center DOAs and 2D angular spreads than an existing estimator.

Index Terms—Incoherently distributed sources, noncircular sources, 2D center DOA estimation, 2D angular spread estimation, generalized shift invariance, rank reduction.

I. INTRODUCTION

As one of the classic localization methods, direction of arrival (DOA) estimation has been widely studied in applications such as robotics, wireless communications, radar and

This work is supported by Key Laboratory of Intelligent Perception and Advanced Control of State Ethnic Affairs Commission under Grant MD-IPAC-2019102, and by Zhejiang Provincial Natural Science Foundation of China under Grants LQ19F010002 and LR20F010001, and by the National Natural Science Foundation of China under Grant 61871282, and by Natural Science Foundation of Ningbo Municipality under Grant 2018A610094, and by K. C. Wong Magna Fund in Ningbo University. (*Corresponding Authors: Qing Wang and Gang Wang*)

Hua Chen is with the Faculty of Electrical Engineering and Computer Science, Ningbo University, Ningbo, 315211, China, and also with the Key Laboratory of Intelligent Perception and Advanced Control of State Ethnic Affairs Commission, Dalian, 116600, China. (e-mail: dkchenhua0714@hotmail.com).

Yonghong Liu and Gang Wang are with Faculty of Information Science and Engineering, Ningbo University, Ningbo, 315211, China. (e-mail: wang-gang@nbu.edu.cn).

Qing Wang is with School of Electronic Informatin Engineering, Tianjin University, Tianjin 300072, China. (e-mail: wqelaine@tju.edu.cn).

Wei Liu is with Department of Electronic and Electrical Engineering, University of Sheffield, Sheffield S1 3JD, UK (e-mail: w.liu@sheffield.ac.uk).

underwater acoustics¹ [1]–[5]. Traditional DOA estimation techniques usually assume a point source model and two representative approaches are the subspace-based [6] and sparse representation-based [7]. However, in many practical scenarios, such as cellular wireless systems, the incoming signals will collide with antenna arrays from different paths of different angles, which corresponds to the multipath transmission and leads to the angular spread phenomenon [8]. Therefore, a distributed source model is more appropriate for such a scenario [8], which is further categorized into coherently distributed (CD) sources and incoherently distributed (ID) sources based on the correlation of the propagation channel to the signal components from different directions, in correspondence to slowly time-varying channels and rapidly time-varying channels, respectively. By extending the classical point source model methods [9]–[14] to CD source model, both center DOA and angle spreads estimations of CD sources have been well studied in the past few decades. However, for the ID source, the rank of its noiseless covariance matrix will increase with the angular spread, and its components occupy the entire observation space, leaving the noise subspace empty. The focus of this paper is to deal with this rather challenging problem.

Currently, many ID source estimators have been developed, such as the estimation of signal parameters via rotational invariance techniques (ESPRIT)-ID algorithm [9], the dispersed signal parameter estimation (DISPARE) algorithm [15], the maximum likelihood (ML) algorithm [16], the covariance matching (COMET) algorithm [17] and some other improvements [18]–[20]. However, the above-mentioned estimators are only limited to the one-dimensional (1D) scenario. In practice, the two-dimensional (2D) angle parameters are more suitable to characterize the actual three-dimensional (3D) space [21]. Since the model of 2D ID sources can be represented by four angular parameters: two center DOAs and two angular spreads, high computational complexity associated with multi-dimensional spectrum search becomes the main problem [15]–[17]. To solve this problem, some 2D ID source parameter estimation algorithms have been developed [21]–[24].

¹In response to one reviewer’s comment about its potential to deal with the current global situation of COVID-19 pandemic, one possible application scenario of the DOA estimation technique is to localize and track the movement of infected patients and high-risk and vulnerable individuals by using array receivers to process the signals transmitted by their carried mobile devices.

Based on the bi-parallel uniform linear arrays (ULAs) and the improved total least squares (TLS)-ESPRIT method, the 2D center DOAs of multiple ID sources can be effectively estimated through 1D search without involving the solutions of the 2D angular spreads [21]. Then, a low-complexity 2D ESPRIT-based approach was proposed to estimate the 2D center DOAs and 2D angular spreads of the ID sources [22], which shows superior performance in massive multiple-input multiple-output (MIMO) systems, evaluated by the derived approximate Cramer-Rao bound (CRB). Subsequently, in [23], a generalized beamspace method, based on a uniform cylindrical array (UCYA) was proposed for 2D localization of ID sources in massive MIMO systems, by reducing the total dimensions of the received signal vectors through beamspace transformation. In order to avoid the spectrum search process in [23], a 2D center DOA estimation algorithm for ID sources in massive MIMO systems was presented in [24] based on a uniform rectangular array (URA), which adopted the beamspace shift invariance structure of total least squares method, and the 2D angular spreads were then obtained in a closed-form solution. However, none of the above studies takes into account the non-circularity property of the signals.

Noncircularity and circularity are important properties of the signal, and their concepts come directly from the geometric interpretation of complex random variables. If the statistical characteristics of the signal has the rotational invariance characteristic, it is called a circular signal; otherwise, it is called a noncircular signal. In wireless communication systems, many widely used modulated signals such as BPSK and AM are noncircular signals, while some other modulated signals such as QAM and QPSK are circular. Owing to the fact that both the conjugated and unconjugated covariance matrices of noncircular signals are non-zero, additional information can be used for estimating the angular parameters by expanding the virtual aperture of the array to improve the performance [25]–[28]. In recent years, some algorithms have been proposed for ID sources by taking advantage of the noncircularity of the signals [29]–[33]. In [29]–[31], the concerned problem mainly focused on estimating the 1D center DOAs of noncircular ID sources, which achieved a superior performance than its circular counterparts. Aiming at 2D noncircular ID sources, a low-complexity 2D center DOA estimation algorithm with automatic pairing was proposed in [32], based on three parallel ULAs, which does not require spectrum search and eigenvalue decomposition, but the solution to the 2D angular spreads was not provided. In the case of coexistence of ID circular and noncircular sources, a conjugate generalized shift invariance algorithm was proposed in [33] based on URAs. A match-pairing method based on a generalized array manifold (GAM) model was designed for such mixed scenarios, and the CRB was also analyzed. However, algorithms for 2D noncircular ID sources are still scarce and further work is needed in this direction.

In this paper, a novel method for joint 2D center DOA and 2D angle spread estimation of noncircular ID sources is proposed based on the extended GAM model using the first-order Taylor series approximation, which focuses on the reduced-rank principle with the noncircularity-based generalized shift

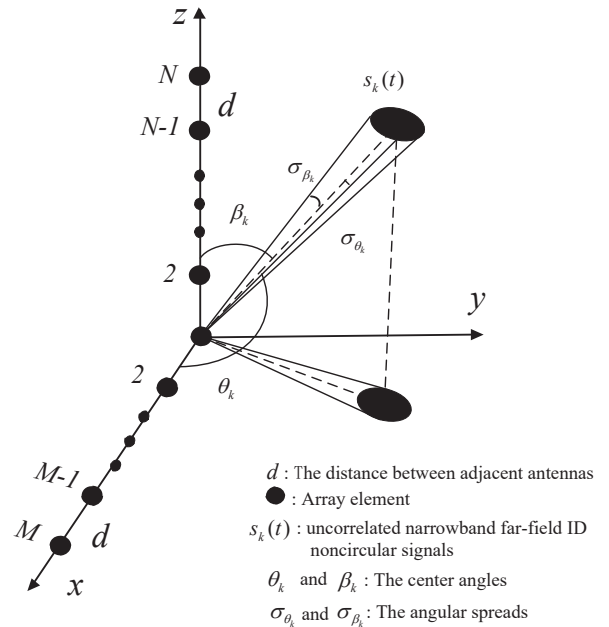


Fig. 1: An L-shaped array structure.

invariance property. The contributions of the paper are given as follows.

- (1) Compared with Cao's algorithm [18], the proposed algorithm exploits the signal's noncircularity information to handle more ID sources with improved estimation accuracy.
- (2) Compared with the multi-dimensional spectrum search method, the proposed method only requires two 1-D spectrum searches to obtain the 2D center DOAs of noncircular ID sources, and the 2D angle spreads are obtained in closed-form solutions.
- (3) The proposed algorithm does not require prior knowledge of the angular distribution; as a result, it can be applied to situations where multiple sources have different angular distributions.
- (4) The approximate stochastic noncircular CRB for joint 2D center DOA and 2D angle spread estimation of noncircular ID sources is derived as a benchmark.

The rest of this paper is organized as follows. Section 2 introduces the general signal model. The proposed algorithm is presented in detail in Section 3. The approximate stochastic CRB of the concerned problem is derived in Section 4. Simulation results are provided in Section 5, followed by conclusions in Section 6. A explanation of notations used is shown in Table I.

II. ARRAY SIGNAL MODEL

Consider an L -shaped array consisting of two crossed ULAs with in total $F = M + N - 1$ elements, where the antenna array on the x axis and the z axis has M and N elements, respectively, as illustrated in Fig. 1. The distance between adjacent antennas d is equal to half-wavelength of incident signals. There are K uncorrelated narrowband far-field ID noncircular signals $s_k(t)$ ($k = 1, 2, \dots, K$) impinging on the array. The center angles $\theta_k \in [0, \pi]$ and $\beta_k \in [0, \pi]$ are from

TABLE I: Explanation of notations.

$(\cdot)^*$: conjugate	$\det\{\cdot\}$: the determinant of a matrix
$(\cdot)^T$: transpose	$\text{tr}\{\cdot\}$: the trace of a matrix
$(\cdot)^{-1}$: inverse	$\text{diag}\{\cdot\}$: diagonal matrix formed by its elements
$(\cdot)^H$: conjugate transpose	$\text{blkdiag}\{\cdot\}$: the generation of a block diagonal matrix
\otimes : Kronecker product	$E\{\cdot\}$: the expectation operation
\odot : Hadamard product	$[\cdot]_{l,k}$: the (l, k) th elements of a matrix
$\mathbf{I}_{k \times k}$: the $k \times k$ identity matrix	$\text{vec}\{\cdot\}$: an operator stacking the columns of a matrix on top of one another
$\mathbf{0}_{k \times l}$: the $k \times l$ zero matrix	$\lfloor \cdot \rfloor$: the floor function, giving the largest integer less than or equal to its input

the x axis and the z axis to the central line, respectively. Thus, the observed signal vectors of the L -shaped array at time t can be expressed as

$$\mathbf{x}(t) = \sum_{k=1}^K s_k(t) \sum_{l=1}^{L_k} \gamma_{k,l}(t) \mathbf{a}(\bar{\theta}_{k,l}, \bar{\beta}_{k,l}) + \mathbf{n}(t) \quad (1)$$

where $t = 1, 2, \dots, T$ is the sampling time, and T is the number of snapshots; L_k is the total number of rays from the k th signal; $\bar{\theta}_{k,l}$ and $\bar{\beta}_{k,l}$ are the 2D DOAs of the l th ray related to the k th signal with the $F \times 1$ array manifold vector $\mathbf{a}(\bar{\theta}_{k,l}, \bar{\beta}_{k,l}) = [e^{j2\pi(N-1)d \cos \bar{\beta}_{k,l}/\lambda}, \dots, e^{j2\pi d \cos \bar{\beta}_{k,l}/\lambda}, 1, e^{j2\pi d \cos \bar{\theta}_{k,l}/\lambda}, \dots, e^{j2\pi(M-1)d \cos \bar{\theta}_{k,l}/\lambda}]^T$; $\gamma_{k,l}(t)$ is the complex-valued gain for the l th ray of the k th signal; $\mathbf{n}(t) = [n_1(t), \dots, n_F(t)]^T$ is the $F \times 1$ additive white Gaussian noise vector with zero mean and covariance σ_n^2 . For ID sources, the ray gains $\gamma_{k,l}(t)$ are assumed to be temporally white and is independent from ray to ray with zero-mean and covariance [18]

$$E\{\gamma_{k,l}(t)\gamma_{k',l'}^*(t')\} = \frac{\sigma_{\gamma_k}^2}{L_k} \delta(k - k')\delta(l - l')\delta(t - t') \quad (2)$$

$\bar{\theta}_{k,l}$ and $\bar{\beta}_{k,l}$ can be represented as

$$\bar{\theta}_{k,l} = \theta_k + \tilde{\theta}_{k,l}(t) \quad (3)$$

$$\bar{\beta}_{k,l} = \beta_k + \tilde{\beta}_{k,l}(t) \quad (4)$$

where θ_k and β_k are the center DOAs of the k th noncircular signal; $\tilde{\theta}_{k,l}(t)$ and $\tilde{\beta}_{k,l}(t)$ are the random angular deviation from the center DOAs θ_k and β_k , which are both assumed to be real-valued zero-mean random variables with variance $\sigma_{\theta_k}^2$ and variance $\sigma_{\beta_k}^2$, respectively. Here, we assume that the value of $\tilde{\theta}_{k,l}(t)$ and $\tilde{\beta}_{k,l}(t)$ is small, i.e., the DOAs from different rays radiated by one noncircular signal are relatively close to each other.

It is also assumed that $\zeta_1 \triangleq \tilde{\theta}_{k,l}(t)$ and $\zeta_2 \triangleq \tilde{\beta}_{k,l}(t)$ are a real-valued zero-mean random variables with probability density function $p_k(\zeta_1, \zeta_2; \sigma_{\theta_k}, \sigma_{\beta_k})$. Moreover, $p_k(\zeta_1, \zeta_2; \sigma_{\theta_k}, \sigma_{\beta_k})$ is generally supposed to be a symmetric function about ζ_1 and ζ_2 , with two typical distributions [32]: the Gaussian distribution

$$p_k(\zeta_1, \zeta_2; \sigma_{\theta_k}, \sigma_{\beta_k}) = \frac{1}{2\pi\sigma_{\theta_k}\sigma_{\beta_k}} \exp\{-\frac{1}{2}(\zeta_1^2/\sigma_{\theta_k}^2 + \zeta_2^2/\sigma_{\beta_k}^2)\} \quad (5)$$

and the uniform distribution

$$p_k(\zeta_1, \zeta_2; \sigma_{\theta_k}, \sigma_{\beta_k}) = \begin{cases} \frac{1}{2\sqrt{3}\sigma_{\theta_k}}, & |\zeta_1| < \sqrt{3}\sigma_{\theta_k} \\ \frac{1}{2\sqrt{3}\sigma_{\beta_k}}, & |\zeta_2| < \sqrt{3}\sigma_{\beta_k} \\ 0, & \text{otherwise.} \end{cases} \quad (6)$$

III. THE PROPOSED ALGORITHM

A. Extended GAM model

With the small angle spread assumption in (3) and (4), the manifold vector $\mathbf{a}(\bar{\theta}_{k,l}, \bar{\beta}_{k,l})$ can be approximated as (7) with the first-order Taylor series expansion [24] around the 2-D nominal DOAs, i.e.,

$$\mathbf{a}(\bar{\theta}_{k,l}, \bar{\beta}_{k,l}) \approx \mathbf{a}(\theta_k, \beta_k) + \mathbf{a}'_{\theta}(\theta_k, \beta_k)\tilde{\theta}_{k,l}(t) + \mathbf{a}'_{\beta}(\theta_k, \beta_k)\tilde{\beta}_{k,l}(t) \quad (7)$$

where $\mathbf{a}'_{\theta}(\theta_k, \beta_k) = \frac{\partial \mathbf{a}(\theta_k, \beta_k)}{\partial \theta_k}$ and $\mathbf{a}'_{\beta}(\theta_k, \beta_k) = \frac{\partial \mathbf{a}(\theta_k, \beta_k)}{\partial \beta_k}$ are the partial derivative of $\mathbf{a}(\theta_k, \beta_k)$ with respect to θ_k and β_k , respectively. Substituting (7) into (1), we have

$$\mathbf{x}(t) \approx \sum_{k=1}^K (\mathbf{a}(\theta_k, \beta_k)v_{k,0}(t) + \mathbf{a}'_{\theta}(\theta_k, \beta_k)v_{k,1}(t) + \mathbf{a}'_{\beta}(\theta_k, \beta_k)v_{k,2}(t)) + \mathbf{n}(t) \quad (8)$$

where

$$\begin{aligned} v_{k,0}(t) &= s_k(t) \sum_{l=1}^{L_k} \gamma_{k,l} \\ v_{k,1}(t) &= s_k(t) \sum_{l=1}^{L_k} \gamma_{k,l} \tilde{\theta}_{k,l}(t) \\ v_{k,2}(t) &= s_k(t) \sum_{l=1}^{L_k} \gamma_{k,l} \tilde{\beta}_{k,l}(t). \end{aligned} \quad (9)$$

Then, we can reformulate (8) into the GAM model as

$$\mathbf{x}(t) \approx \mathbf{B}(\theta, \beta)\mathbf{g}(t) + \mathbf{n}(t) \quad (10)$$

and the GAM matrix $\mathbf{B}(\theta, \beta)$ depends only on the center DOAs, where

$$\mathbf{B}(\theta, \beta) = [\mathbf{A}(\theta_1, \beta_1), \mathbf{A}(\theta_2, \beta_2), \dots, \mathbf{A}(\theta_K, \beta_K)] \in C^{F \times 3K} \quad (11)$$

$$\mathbf{A}(\theta_k, \beta_k) = [\mathbf{a}(\theta_k, \beta_k), \mathbf{a}'_{\theta}(\theta_k, \beta_k), \mathbf{a}'_{\beta}(\theta_k, \beta_k)] \in C^{F \times 3} \quad (12)$$

$$\mathbf{g}(t) = [\mathbf{g}_1^T, \mathbf{g}_2^T, \dots, \mathbf{g}_K^T]^T \in C^{3K \times 1} \quad (13)$$

$$\mathbf{g}_k = [v_{k,0}(t), v_{k,1}(t), v_{k,2}(t)] \in C^{3 \times 1}. \quad (14)$$

Due to the common assumption that the transmitted signals, the path gains, and the angular deviations are mutually uncorrelated with each other [18], the variance of $v_{k,1}(t)$ and

$v_{k,2}(t)$ can be expressed as

$$\begin{aligned} E \left\{ v_{k,1}(t)v_{k,1}^*(t) \right\} &= \rho_k \sigma_{\theta_k}^2 \\ E \left\{ v_{k,2}(t)v_{k,2}^*(t) \right\} &= \rho_k \sigma_{\beta_k}^2 \end{aligned} \quad (15)$$

where $\rho_k = E \{ |s_k(t)|^2 \} \sigma_k^2$ is the power of the k th noncircular signal. Additionally, the variance of $v_{k,0}(t)$ is

$$E \{ v_{k,0}(t)v_{k,0}^*(t) \} = \rho_k \quad (16)$$

and also we have

$$E \{ v_{k,n}(t)v_{k',n'}^*(t) \} = 0, \forall k \neq k' \text{ or } n \neq n'. \quad (17)$$

From (15), (16), and (17), the covariance matrix of $\mathbf{g}(t)$ can be expressed as

$$\mathbf{\Lambda} = E \{ \mathbf{g}(t)\mathbf{g}^H(t) \} = \text{blkdiag} \{ \mathbf{\Lambda}_1, \mathbf{\Lambda}_2, \dots, \mathbf{\Lambda}_K \} \quad (18)$$

where $\mathbf{\Lambda}_k = \rho_k \text{diag} \{ 1, \sigma_{\theta_k}^2, \sigma_{\beta_k}^2 \} (k = 1, 2, \dots, K)$.

Using the noncircularity characteristics of the signal can increase the a priori information, so it can also greatly improve the estimation performance of DOA to some extent. Here, we only consider the rotation invariance characteristics of the signal. For a complex random signals s_k , we define $E\{s_k\}$, $E\{s_k s_k^*\}$ and $E\{s_k^2\}$ as the mean, covariance and ellipse covariance of the signal s_k , respectively. If the first and second order statistical characteristics of the signal are not rotational invariant for an arbitrary phase φ_k as follows [28]

$$\begin{aligned} E\{s_k e^{j\varphi_k}\} &\neq E\{s_k\} \\ E\{s_k e^{j\varphi_k} (s_k e^{j\varphi_k})^*\} &= E\{s_k s_k^*\} \\ E\{s_k e^{j\varphi_k} \cdot s_k e^{j\varphi_k}\} &\neq E\{s_k^2\} \end{aligned} \quad (19)$$

the signal s_k will be called a noncircular signal. For simplicity, the emitted signals are supposed to be strictly noncircular with the maximal noncircularity rate. Thus, $\mathbf{g}(t)$ can be re-expressed as [32]

$$\mathbf{g}(t) = \mathbf{\Phi} \mathbf{g}_0(t) \quad (20)$$

where $\mathbf{g}_0(t) \in C^{3K \times 1}$ is the real-valued signal vector; $\mathbf{\Phi} = \text{diag} \{ e^{j\omega_1}, e^{j\omega'_{\theta,1}}, e^{j\omega'_{\beta,1}}, \dots, e^{j\omega_K}, e^{j\omega'_{\theta,K}}, e^{j\omega'_{\beta,K}} \}$ is a $3K \times 3K$ diagonal matrix, which contains the noncircular phase information in each element of the vector $\omega = [\omega_1, \omega'_{\theta,1}, \omega'_{\beta,1}, \dots, \omega_K, \omega'_{\theta,K}, \omega'_{\beta,K}]^T$.

In order to exploit the noncircularity information of the strictly noncircular signals, a new data vector can be written by concatenating the original data vector $\mathbf{x}(t)$ and its conjugate counterpart as

$$\begin{aligned} \mathbf{y}(t) &= \begin{bmatrix} \mathbf{x}(t) \\ \mathbf{x}^*(t) \end{bmatrix} = \begin{bmatrix} \mathbf{B}(\theta, \beta) \mathbf{g}(t) \\ \mathbf{B}^*(\theta, \beta) \mathbf{g}^*(t) \end{bmatrix} + \begin{bmatrix} \mathbf{n}(t) \\ \mathbf{n}^*(t) \end{bmatrix} \\ &= \begin{bmatrix} \mathbf{B}(\theta, \beta) \\ \mathbf{B}^*(\theta, \beta) \mathbf{\Phi}^{-2} \end{bmatrix} \mathbf{g}(t) + \begin{bmatrix} \mathbf{n}(t) \\ \mathbf{n}^*(t) \end{bmatrix} \\ &= \mathbf{B}(\theta, \beta) \mathbf{g}(t) + \bar{\mathbf{n}}(t) \end{aligned} \quad (21)$$

where

$$\bar{\mathbf{B}}(\theta, \beta) = \begin{bmatrix} \mathbf{B}(\theta, \beta) \\ \mathbf{B}^*(\theta, \beta) \mathbf{\Phi}^{-2} \end{bmatrix} \in C^{2F \times 3K} \quad (22)$$

is the extended GAM matrix; $\bar{\mathbf{n}}(t) = \begin{bmatrix} \mathbf{n}(t) \\ \mathbf{n}^*(t) \end{bmatrix} \in C^{2F \times 1}$ is

the extended noise matrix.

The covariance matrix of the extended data vector $\mathbf{y}(t)$ is given by

$$\mathbf{R} = E \{ \mathbf{y}(t)\mathbf{y}^H(t) \} = \bar{\mathbf{B}}(\theta, \beta) \mathbf{\Lambda} \bar{\mathbf{B}}^H(\theta, \beta) + \sigma_n^2 \mathbf{I}_{2F} \quad (23)$$

where $\mathbf{\Lambda}$ is the covariance matrix of $\mathbf{g}(t)$.

By performing eigenvalue decomposition (EVD) on \mathbf{R} , we have

$$\mathbf{R} = \mathbf{U}_s \mathbf{\Sigma}_s \mathbf{U}_s^H + \mathbf{U}_n \mathbf{\Sigma}_n \mathbf{U}_n^H \quad (24)$$

where the $2F \times 3K$ matrix \mathbf{U}_s is the signal subspace corresponding to diagonal matrix $\mathbf{\Sigma}_s$ composed of $3K$ large eigenvalues, and the $2F \times (2F - 3K)$ matrix \mathbf{U}_n is the noise subspace corresponding to diagonal matrix $\mathbf{\Sigma}_n$ composed of $(2F - 3K)$ small eigenvalues.

B. Estimation of Center DOAs

To obtain the 2D center DOA estimates, the sensor array on the x axis and the z axis is divided into two subarrays with equivalent number of sensors. To ensure estimation accuracy, we set $M_1 = M - 1$ and $N_1 = N - 1$ to be the number of sensors of each subarray on the x axis and the z axis, respectively. Then we have four subarrays with the sensor elements indexed as $\{x_1, \dots, x_{M-1}\}$, $\{x_2, \dots, x_M\}$, $\{z_1, \dots, z_{N-1}\}$ and $\{z_2, \dots, z_N\}$, respectively. For simplicity, $\{x_{1,m}\}_{m=1}^{M_1}$ and $\{x_{2,m}\}_{m=1}^{M_1}$ denote the locations of the sensors in each subarray along the x axis, respectively; $\{z_{1,n}\}_{n=1}^{N_1}$ and $\{z_{2,n}\}_{n=1}^{N_1}$ denote the locations of the sensors in each subarray along the z axis, respectively, where $x_{1,m} < x_{2,m} (m = 1, \dots, M_1)$, $z_{1,n} < z_{2,n} (n = 1, \dots, N_1)$.

Define the following four selection matrices

$$\mathbf{J}_1 = [\mathbf{0}_{M_1 \times N_1} \quad \mathbf{I}_{M_1} \quad \mathbf{0}_{M_1 \times 1}] \in C^{M_1 \times F} \quad (25)$$

$$\mathbf{J}_2 = [\mathbf{0}_{M_1 \times N_1} \quad \mathbf{0}_{M_1 \times 1} \quad \mathbf{I}_{M_1}] \in C^{M_1 \times F} \quad (26)$$

$$\mathbf{J}_3 = [\mathbf{0}_{N_1 \times 1} \quad \mathbf{I}_{N_1} \quad \mathbf{0}_{N_1 \times M_1}] \in C^{N_1 \times F} \quad (27)$$

$$\mathbf{J}_4 = [\mathbf{I}_{N_1} \quad \mathbf{0}_{N_1 \times 1} \quad \mathbf{0}_{N_1 \times M_1}] \in C^{N_1 \times F}. \quad (28)$$

With (11), (12) and (22), we have

$$\mathbf{K}_2 \bar{\mathbf{a}}(\theta_k, \beta_k) = \mathbf{\Omega}_k \mathbf{K}_1 \bar{\mathbf{a}}(\theta_k, \beta_k) \quad (29)$$

$$\mathbf{K}_2 \bar{\mathbf{a}}'_\theta(\theta_k, \beta_k) = \mathbf{\Omega}'_{\theta,k} \mathbf{K}_1 \bar{\mathbf{a}}'_\theta(\theta_k, \beta_k) \quad (30)$$

$$\mathbf{K}_2 \bar{\mathbf{a}}'_\beta(\theta_k, \beta_k) = \mathbf{\Omega}'_{\beta,k} \mathbf{K}_1 \bar{\mathbf{a}}'_\beta(\theta_k, \beta_k) \quad (31)$$

where

$$\bar{\mathbf{a}}(\theta_k, \beta_k) = \begin{bmatrix} \mathbf{a}(\theta_k, \beta_k) \\ e^{-j2\omega_k} \mathbf{a}^*(\theta_k, \beta_k) \end{bmatrix} \in C^{2F \times 1} \quad (32)$$

$$\bar{\mathbf{a}}'_\theta(\theta_k, \beta_k) = \begin{bmatrix} \mathbf{a}'_\theta(\theta_k, \beta_k) \\ e^{-j2\omega'_{\theta,k}} \mathbf{a}'_{\theta,*}(\theta_k, \beta_k) \end{bmatrix} \in C^{2F \times 1} \quad (33)$$

$$\bar{\mathbf{a}}'_\beta(\theta_k, \beta_k) = \begin{bmatrix} \mathbf{a}'_\beta(\theta_k, \beta_k) \\ e^{-j2\omega'_{\beta,k}} \mathbf{a}'_{\beta,*}(\theta_k, \beta_k) \end{bmatrix} \in C^{2F \times 1} \quad (34)$$

$$\mathbf{\Omega}_k = \text{blkdiag} \{ e^{j\phi_k} \mathbf{I}_{M_1}, e^{-j\phi_k} \mathbf{I}_{M_1} \}, \phi_k = 2\pi d \cos \theta_k / \lambda \quad (35)$$

$$\mathbf{\Omega}'_{\theta,k} = \text{diag} \{ \varepsilon_1 e^{j\phi_k}, \dots, \varepsilon_{M_1} e^{j\phi_k}, \varepsilon_1 e^{-j\phi_k}, \dots, \varepsilon_{M_1} e^{-j\phi_k} \}, \varepsilon_m = \frac{x_{2,m}}{x_{1,m}} \quad (36)$$

$$\mathbf{\Omega}'_{\beta,k} = \mathbf{0}_{2M_1 \times 2M_1} \quad (37)$$

$\mathbf{a}(\theta_k, \beta_k) = [e^{j2\pi N_1 d \cos \beta_{k,i}/\lambda}, \dots, e^{j2\pi d \cos \beta_{k,i}/\lambda}, 1, e^{j2\pi d \cos \theta_{k,i}/\lambda}, \dots, e^{j2\pi M_1 d \cos \theta_{k,i}/\lambda}]^T$ is an $F \times 1$ vector; $\mathbf{a}^*(\theta_k, \beta_k)$, $\mathbf{a}'_{\theta}(\theta_k, \beta_k)$ and $\mathbf{a}'_{\beta}(\theta_k, \beta_k)$ are the conjugate of $\mathbf{a}(\theta_k, \beta_k)$, $\mathbf{a}'_{\theta}(\theta_k, \beta_k)$ and $\mathbf{a}'_{\beta}(\theta_k, \beta_k)$, respectively; $\mathbf{K}_1 = \text{blkdiag}\{\mathbf{J}_1, \mathbf{J}_1\}$, $\mathbf{K}_2 = \text{blkdiag}\{\mathbf{J}_2, \mathbf{J}_2\}$. From (29), (30) and (31), it can be obtained that

$$\bar{\mathbf{B}}(\theta_k, \beta_k) = [\bar{\mathbf{a}}(\theta_k, \beta_k), \bar{\mathbf{a}}'_{\theta}(\theta_k, \beta_k), \bar{\mathbf{a}}'_{\beta}(\theta_k, \beta_k)] \quad (38)$$

$$\begin{aligned} \mathbf{K}_2 \bar{\mathbf{B}}(\theta, \beta) = & [\mathbf{\Omega}_1 \mathbf{K}_1 \bar{\mathbf{a}}(\theta_1, \beta_1), \mathbf{\Omega}'_{\theta,1} \mathbf{K}_1 \bar{\mathbf{a}}'_{\theta}(\theta_1, \beta_1), \\ & \mathbf{\Omega}'_{\beta,1} \mathbf{K}_1 \bar{\mathbf{a}}'_{\beta}(\theta_1, \beta_1), \dots, \mathbf{\Omega}_K \mathbf{K}_1 \bar{\mathbf{a}}(\theta_K, \beta_K), \\ & \mathbf{\Omega}'_{\theta,K} \mathbf{K}_1 \bar{\mathbf{a}}'_{\theta}(\theta_K, \beta_K), \mathbf{\Omega}'_{\beta,K} \mathbf{K}_1 \bar{\mathbf{a}}'_{\beta}(\theta_K, \beta_K)] \end{aligned} \quad (39)$$

It is noted that \mathbf{U}_s has the same column space as the GAM matrix $\bar{\mathbf{B}}(\theta, \beta)$, which has the form of

$$\mathbf{U}_s = \bar{\mathbf{B}}(\theta, \beta) \mathbf{T} \quad (40)$$

where \mathbf{T} is an invertible $3K \times 3K$ matrix.

Similarly, two submatrices $\mathbf{U}_1 \in C^{2M_1 \times 3K}$ and $\mathbf{U}_2 \in C^{2M_1 \times 3K}$ can be extracted from \mathbf{U}_s , corresponding to the partition of the two subarrays on the axis, namely,

$$\mathbf{U}_1 = \mathbf{K}_1 \mathbf{U}_s = \mathbf{K}_1 \bar{\mathbf{B}}(\theta, \beta) \mathbf{T} \quad (41)$$

$$\mathbf{U}_2 = \mathbf{K}_2 \mathbf{U}_s = \mathbf{K}_2 \bar{\mathbf{B}}(\theta, \beta) \mathbf{T}. \quad (42)$$

To proceed, we define a new matrix $\Psi(\theta)$ as

$$\Psi(\theta) = \text{blkdiag}\{e^{j\psi} \mathbf{I}_{M_1}, e^{-j\psi} \mathbf{I}_{M_1}\} \quad (43)$$

where $\psi = 2\pi d \sin \theta / \lambda$. Then, we formulate a matrix $\mathbf{D}(\theta)$ as

$$\mathbf{D}(\theta) = \mathbf{U}_2 - \Psi(\theta) \mathbf{U}_1 = (\mathbf{K}_2 \bar{\mathbf{B}} - \Psi(\theta) \mathbf{K}_1 \bar{\mathbf{B}}) \mathbf{T} = \mathbf{Q}(\theta) \mathbf{T} \quad (44)$$

where $\mathbf{Q}(\theta) = (\mathbf{K}_2 \bar{\mathbf{B}} - \Psi(\theta) \mathbf{K}_1 \bar{\mathbf{B}})$. Resorting to (39), $\mathbf{Q}(\theta)$ can be rewritten as

$$\begin{aligned} \mathbf{Q}(\theta) = & [(\mathbf{\Omega}_1 - \Psi(\theta)) \mathbf{K}_1 \bar{\mathbf{a}}(\theta_1, \beta_1), (\mathbf{\Omega}'_{\theta,1} - \Psi(\theta)) \mathbf{K}_1 \bar{\mathbf{a}}'_{\theta}(\theta_1, \beta_1), \\ & (\mathbf{\Omega}'_{\beta,1} - \Psi(\theta)) \mathbf{K}_1 \bar{\mathbf{a}}'_{\beta}(\theta_1, \beta_1), \dots, (\mathbf{\Omega}_K - \Psi(\theta)) \mathbf{K}_1 \\ & \times \bar{\mathbf{a}}(\theta_K, \beta_K), (\mathbf{\Omega}'_{\theta,K} - \Psi(\theta)) \mathbf{K}_1 \bar{\mathbf{a}}'_{\theta}(\theta_K, \beta_K), \\ & (\mathbf{\Omega}'_{\beta,K} - \Psi(\theta)) \mathbf{K}_1 \bar{\mathbf{a}}'_{\beta}(\theta_K, \beta_K)] \end{aligned} \quad (45)$$

It can be seen in (45) that when $\theta = \theta_k$, all the elements of $(\mathbf{\Omega}_k - \Psi(\theta))$ become zero. Therefore, if $K \leq M_1$, then $\mathbf{D}(\theta)$ is rank deficient and the determinant of $\mathbf{D}^H(\theta) \mathbf{D}(\theta)$ is zero. The center angles $\{\hat{\theta}_k\}_{k=1}^K$ can be obtained by searching for peaks of the following function

$$f(\theta) = \frac{1}{\det\{\mathbf{D}^H(\theta) \mathbf{D}(\theta)\}}. \quad (46)$$

To estimate the center angle β , similarly we extract two submatrices $\mathbf{U}_3 \in C^{2N_1 \times 3K}$ and $\mathbf{U}_4 \in C^{2N_1 \times 3K}$ from \mathbf{U}_s , which correspond to the partition of the two subarrays on the Z axis,

$$\mathbf{U}_3 = \mathbf{K}_3 \mathbf{U}_s = \mathbf{K}_3 \bar{\mathbf{B}}(\theta, \beta) \mathbf{T} \quad (47)$$

$$\mathbf{U}_4 = \mathbf{K}_4 \mathbf{U}_s = \mathbf{K}_4 \bar{\mathbf{B}}(\theta, \beta) \mathbf{T} \quad (48)$$

where $\mathbf{K}_3 = \text{blkdiag}\{\mathbf{J}_3, \mathbf{J}_3\}$, and $\mathbf{K}_4 = \text{blkdiag}\{\mathbf{J}_4, \mathbf{J}_4\}$.

Define a matrix $\Psi(\beta)$ as

$$\Psi(\beta) = \text{blkdiag}\{e^{j\psi} \mathbf{I}_{N_1}, e^{-j\psi} \mathbf{I}_{N_1}\} \quad (49)$$

where $\psi = 2\pi d \cos \beta / \lambda$. Then, we formulate $\mathbf{D}(\beta)$ as

$$\mathbf{D}(\beta) = \mathbf{U}_4 - \Psi(\beta) \mathbf{U}_3 = (\mathbf{K}_4 \bar{\mathbf{B}} - \Psi(\beta) \mathbf{K}_3 \bar{\mathbf{B}}) \mathbf{T} = \mathbf{Q}(\beta) \mathbf{T} \quad (50)$$

where $\mathbf{Q}(\beta) = (\mathbf{K}_4 \bar{\mathbf{B}} - \Psi(\beta) \mathbf{K}_3 \bar{\mathbf{B}})$. Similarly, $\mathbf{Q}(\beta)$ can be rewritten as

$$\begin{aligned} \mathbf{Q}(\beta) = & [(\mathbf{\Theta}_1 - \Psi(\beta)) \mathbf{K}_1 \bar{\mathbf{a}}(\theta_1, \beta_1), (\mathbf{\Theta}'_{\theta,1} - \Psi(\beta)) \mathbf{K}_1 \bar{\mathbf{a}}'_{\theta}(\theta_1, \beta_1), \\ & (\mathbf{\Theta}'_{\beta,1} - \Psi(\beta)) \mathbf{K}_1 \bar{\mathbf{a}}'_{\beta}(\theta_1, \beta_1), \dots, (\mathbf{\Theta}_K - \Psi(\beta)) \mathbf{K}_1 \\ & \times \bar{\mathbf{a}}(\theta_K, \beta_K), (\mathbf{\Theta}'_{\theta,K} - \Psi(\beta)) \mathbf{K}_1 \bar{\mathbf{a}}'_{\theta}(\theta_K, \beta_K), \\ & (\mathbf{\Theta}'_{\beta,K} - \Psi(\beta)) \mathbf{K}_1 \bar{\mathbf{a}}'_{\beta}(\theta_K, \beta_K)] \end{aligned} \quad (51)$$

where

$$\mathbf{\Theta}_k = \text{blkdiag}\{e^{j\phi_k} \mathbf{I}_{N_1}, e^{-j\phi_k} \mathbf{I}_{N_1}\}, \phi_k = 2\pi d \cos \beta_k / \lambda \quad (52)$$

$$\mathbf{\Theta}'_{\theta,k} = \mathbf{0}_{2N_1 \times 2N_1} \quad (53)$$

$$\begin{aligned} \mathbf{\Theta}'_{\beta,k} = & \text{diag}\{\varepsilon_1 e^{j\phi_k}, \dots, \varepsilon_{N_1} e^{j\phi_k}, \varepsilon_1 e^{-j\phi_k}, \\ & \dots, \varepsilon_{N_1} e^{-j\phi_k}\}, \varepsilon_n = \frac{z_{2,n}}{z_{1,n}}. \end{aligned} \quad (54)$$

It can be seen in (51) that when $\beta = \beta_k$, all the elements of $(\mathbf{\Theta}_k - \Psi(\beta))$ become zero. Therefore, if $K \leq N_1$, then $\mathbf{D}(\beta)$ is rank deficient and the determinant of $\mathbf{D}^H(\beta) \mathbf{D}(\beta)$ is zero. The values of $\{\hat{\beta}_k\}_{k=1}^K$ can be obtained by searching for the peaks of the following function

$$f(\beta) = \frac{1}{\det\{\mathbf{D}^H(\beta) \mathbf{D}(\beta)\}}. \quad (55)$$

C. Angular Spread Estimation

Once obtaining the 2D nominal DOA estimates in (46) and (55), $\mathbf{\Lambda}$ can be estimated from (23) as

$$\hat{\mathbf{\Lambda}} = \bar{\mathbf{B}}(\hat{\theta}, \hat{\beta})^+ (\hat{\mathbf{R}} - \hat{\sigma}_n^2 \mathbf{I}_{2F}) (\bar{\mathbf{B}}^H(\hat{\theta}, \hat{\beta}))^+ \quad (56)$$

where $\bar{\mathbf{B}}(\hat{\theta}, \hat{\beta})$ is the estimate of $\bar{\mathbf{B}}(\theta, \beta)$ by substituting the estimates of θ and β into (22). In addition, the variance $\hat{\sigma}_n^2$ of the noise can be estimated by the average of the $(2F - 3K)$ smallest eigenvalues of $\hat{\mathbf{R}}$. With the expression of $\mathbf{\Lambda}$ in (18), the 2D angular spreads $\hat{\sigma}_{\theta_k}$ and $\hat{\sigma}_{\beta_k}$ can be calculated respectively as

$$\hat{\sigma}_{\theta_k} = \sqrt{\frac{1}{2} \left(\frac{[\hat{\mathbf{\Lambda}}]_{3k-1, 3k-1}}{[\hat{\mathbf{\Lambda}}]_{3k-2, 3k-2}} + \frac{[\hat{\mathbf{\Lambda}}]_{3K+3k-1, 3K+3k-1}}{[\hat{\mathbf{\Lambda}}]_{3K+3k-2, 3K+3k-2}} \right)} \quad (57)$$

$$\hat{\sigma}_{\beta_k} = \sqrt{\frac{1}{2} \left(\frac{[\hat{\mathbf{\Lambda}}]_{3k, 3k}}{[\hat{\mathbf{\Lambda}}]_{3k-2, 3k-2}} + \frac{[\hat{\mathbf{\Lambda}}]_{3K+3k, 3K+3k}}{[\hat{\mathbf{\Lambda}}]_{3K+3k-2, 3K+3k-2}} \right)} \quad (58)$$

where $k = 1, 2, \dots, K$.

D. Pair-Matching Procedure

In the case of a single source, the estimated $\hat{\theta}_k$ and $\hat{\beta}_k$ can be obtained by the above methods, respectively. However, since the estimation of the center angles θ and β is performed

TABLE II: Summary of the proposed algorithm.

Algorithm: Estimation of center DOAs and angular spreads of ID noncircular sources

Step 1 Form the extended data vector $\mathbf{y}(t)$ according to (20);

Step 2 Compute the covariance matrix $\hat{\mathbf{R}}$ via (22), and perform EVD on $\hat{\mathbf{R}}$ to obtain $\hat{\mathbf{U}}_s$;

Step 3 Extract four submatrices $\mathbf{U}_1, \mathbf{U}_2, \mathbf{U}_3$ and \mathbf{U}_4 from \mathbf{U}_s , and formulate matrix $\mathbf{D}(\theta)$ and $\mathbf{D}(\beta)$;

Step 4 Estimate the center DOAs $\hat{\theta}$ and $\hat{\beta}$ through peak searching of (45) and (54);

Step 5 Match $\hat{\theta}$ and $\hat{\beta}$ according to (58);

Step 6 Calculate $\hat{\mathbf{A}}$ via (55) and estimate the angular spreads with (56) and (57).

independently, with multiple incident sources, $\hat{\theta}_k$ and $\hat{\beta}_k$ may not be in a one-to-one correspondence, so they need to be paired. Thus, we substitute $\hat{\theta}_k$ and $\hat{\beta}_k$ into the 2-D MUSIC spatial spectrum to complete the pairing by finding the minimum value of the denominator which can be represented as

$$(\hat{\theta}_k, \hat{\beta}_k) = \arg \min_{\theta, \beta} \left\| \mathbf{E}_n^H \mathbf{a}(\hat{\theta}, \hat{\beta}) \right\|^2 \quad (59)$$

where \mathbf{E}_n is the noise subspace of the covariance matrix of the data vector $\mathbf{x}(t)$, $\|\cdot\|^2$ denotes the l_2 -norm. It is worth noting that the angular spreads $\hat{\sigma}_{\theta_k}$ and $\hat{\sigma}_{\beta_k}$ are automatically paired without any extra processing. The proposed algorithm for estimating the 2D angular parameters of ID noncircular sources is summarized in Table II.

IV. THE APPROXIMATE CRAMER-RAO BOUND

It is well known that the CRB for angular parameter estimation provides a benchmark to evaluate the performance of an unbiased estimator [32]–[34]. In this section, the approximate stochastic noncircular CRB for the unknown angular parameters of ID sources is derived. We start by defining a vector $\boldsymbol{\eta}$ containing all the parameters of interest as

$$\boldsymbol{\eta} = [\boldsymbol{\mu}^T, \mathbf{v}^T]^T \in C^{(6K+1) \times 1} \quad (60)$$

where $\boldsymbol{\mu} = [\boldsymbol{\theta}^T, \boldsymbol{\sigma}_{\theta}^T, \boldsymbol{\beta}^T, \boldsymbol{\sigma}_{\beta}^T]^T \in C^{4K \times 1}$ with $\boldsymbol{\theta} = [\theta_1, \theta_2, \dots, \theta_K]^T$, $\boldsymbol{\beta} = [\beta_1, \beta_2, \dots, \beta_K]^T$, $\boldsymbol{\sigma}_{\theta} = [\sigma_{\theta 1}, \sigma_{\theta 2}, \dots, \sigma_{\theta K}]^T$ and $\boldsymbol{\sigma}_{\beta} = [\sigma_{\beta 1}, \sigma_{\beta 2}, \dots, \sigma_{\beta K}]^T$, and $\mathbf{v} = [\boldsymbol{\psi}^T, \boldsymbol{\rho}^T, \boldsymbol{\sigma}_n^2]^T \in C^{(2K+1) \times 1}$ with the noncircular phase vector $\boldsymbol{\psi} = [\varphi_1, \varphi_2, \dots, \varphi_K]^T$ and $\boldsymbol{\rho} = [\rho_1, \rho_2, \dots, \rho_K]^T$.

Then, with the assumption of small angular spreads, the array manifold $\mathbf{a}(\hat{\theta}_{k,l}, \hat{\beta}_{k,l})$ in (1) can be approximated with the aid of Taylor series expansion as

$$\begin{aligned} & \mathbf{a}(\hat{\theta}_{k,l}, \hat{\beta}_{k,l}) \\ & \approx [e^{j2\pi(N-1)d(\cos \beta_k - \hat{\beta}_{k,l} \sin \beta_k)/\lambda}, \dots, e^{j2\pi d(\cos \beta_k - \hat{\beta}_{k,l} \sin \beta_k)/\lambda} \\ & 1, e^{j2\pi d(\cos \theta_k - \hat{\theta}_{k,l} \sin \theta_k)/\lambda}, \dots, e^{j2\pi(M-1)d(\cos \theta_k - \hat{\theta}_{k,l} \sin \theta_k)/\lambda}]^T. \end{aligned} \quad (61)$$

where $\mathbf{h} = \text{vec}\{\mathbf{R}\}$.

The approximated formulas for the conjugated and unconjugated covariance matrix \mathbf{R}_1 and \mathbf{R}'_1 of the observation are given by [22]

$$\mathbf{R}_1 \approx \sum_{k=1}^K \rho_k \mathbf{R}_s(\theta_k, \sigma_{\theta k}, \beta_k, \sigma_{\beta k}) + \sigma_n^2 \mathbf{I}_M \quad (62)$$

$$\mathbf{R}'_1 \approx \sum_{k=1}^K \rho_k e^{j\varphi_k} \mathbf{R}'_s(\theta_k, \sigma_{\theta k}, \beta_k, \sigma_{\beta k}) \quad (63)$$

where $\mathbf{R}_s(\theta_k, \sigma_{\theta k}, \beta_k, \sigma_{\beta k}) = \mathbf{a}(\theta_k, \beta_k) \mathbf{a}^H(\theta_k, \beta_k) \odot \mathbf{G}(\theta_k, \sigma_{\theta k}, \beta_k, \sigma_{\beta k})$ and $\mathbf{R}'_s(\theta_k, \sigma_{\theta k}, \beta_k, \sigma_{\beta k}) = \mathbf{a}(\theta_k, \beta_k) \mathbf{a}^T(\theta_k, \beta_k) \odot \mathbf{G}'(\theta_k, \sigma_{\theta k}, \beta_k, \sigma_{\beta k})$. Here we make the assumption that the angular distributed functions follow a Gaussian function. The (p, q) th element of $\mathbf{G}(\theta_k, \sigma_{\theta k}, \beta_k, \sigma_{\beta k})$ is given by [22], [32]

$$\begin{aligned} & [\mathbf{G}(\theta_k, \sigma_{\theta k}, \beta_k, \sigma_{\beta k})]_{p,q} \\ & = \exp \left[-0.5 \left(\left(\frac{2\pi}{\lambda} (x_p - x_q) \sigma_{\theta k} \cos \theta_k \right)^2 \right. \right. \\ & \quad \left. \left. + \left(\frac{2\pi}{\lambda} (z_p - z_q) \sigma_{\beta k} \cos \beta_k \right)^2 \right) \right] \end{aligned} \quad (64)$$

and the (p, q) th element of $\mathbf{G}'(\theta_k, \sigma_{\theta k}, \beta_k, \sigma_{\beta k})$ is given by

$$\begin{aligned} & [\mathbf{G}'(\theta_k, \sigma_{\theta k}, \beta_k, \sigma_{\beta k})]_{p,q} \\ & = \exp \left[-0.5 \left(\left(\frac{2\pi}{\lambda} (x_p + x_q - 2) \sigma_{\theta k} \cos \theta_k \right)^2 \right. \right. \\ & \quad \left. \left. + \left(\frac{2\pi}{\lambda} (z_p + z_q - 2) \sigma_{\beta k} \cos \beta_k \right)^2 \right) \right]. \end{aligned} \quad (65)$$

Taking into account the noncircularity of the incoming signals, the extended covariance matrix \mathbf{R} can be further rewritten as

$$\mathbf{R} = \begin{bmatrix} \mathbf{R}_1 & \mathbf{R}'_1 \\ \mathbf{R}'_1^* & \mathbf{R}_1^* \end{bmatrix}. \quad (66)$$

The CRB of $\boldsymbol{\eta}$ can be calculated as [22], [32]–[34]

$$\text{CRB}(\boldsymbol{\eta}) = \mathbf{F}^{-1} \quad (67)$$

where \mathbf{F} is the Fisher information matrix (FIM) with the (p, q) th entry defined as

$$[\mathbf{F}]_{p,q} = \frac{T}{2} \text{tr} \left\{ \mathbf{R}^{-1} \frac{\partial \mathbf{R}}{\partial \boldsymbol{\eta}_p} \mathbf{R}^{-1} \frac{\partial \mathbf{R}}{\partial \boldsymbol{\eta}_q} \right\}. \quad (68)$$

Furthermore, (68) can be rewritten as

$$\frac{2}{T} \mathbf{F} = \left(\frac{\partial \mathbf{h}}{\partial \boldsymbol{\eta}^T} \right)^H (\mathbf{R}^{-T} \otimes \mathbf{R}^{-1}) \left(\frac{\partial \mathbf{h}}{\partial \boldsymbol{\eta}} \right) \quad (69)$$

$$\left(\mathbf{R}^{-T/2} \otimes \mathbf{R}^{-1/2} \right) \left[\frac{\partial \mathbf{h}}{\partial \boldsymbol{\mu}^T} \middle| \frac{\partial \mathbf{h}}{\partial \mathbf{v}^T} \right] \triangleq [\mathbf{U} | \mathbf{V}] \quad (70)$$

where

$$\begin{aligned} & \mathbf{U} \\ & = \left(\mathbf{R}^{-T/2} \otimes \mathbf{R}^{-1/2} \right) \left[\frac{\partial \mathbf{h}}{\partial \boldsymbol{\theta}^T} \middle| \frac{\partial \mathbf{h}}{\partial \boldsymbol{\beta}^T} \middle| \frac{\partial \mathbf{h}}{\partial \boldsymbol{\sigma}_{\theta}^T} \middle| \frac{\partial \mathbf{h}}{\partial \boldsymbol{\sigma}_{\beta}^T} \right] \\ & = [\mathbf{U}_{\theta} | \mathbf{U}_{\beta} | \mathbf{U}_{\sigma_{\theta}} | \mathbf{U}_{\sigma_{\beta}}] \end{aligned} \quad (71)$$

TABLE III: Comparison of the performance by the two algorithms.

Algorithm	Complexity	Maximum number of signals distinguished	Noncircularity used
Proposed	$O((2F)^2T + (2F)^3 + 8FK^2 + 2(2F)^2K + \Delta_\theta(8M_1K^2 + 16M_1^2K) + \Delta_\beta(8N_1K^2 + 16N_1^2K))$	$\min\{M_1, N_1\}$	yes
Cao [18]	$O(F^2T + F^3 + 4FK^2 + 2F^2K + \Delta_\theta(4M_1K^2 + 8M_1^2K) + \Delta_\beta(4N_1K^2 + 8N_1^2K))$	$\lfloor \min\{M_1, N_1\}/2 \rfloor$	no

$$\begin{aligned} \mathbf{V} &= \left(\mathbf{R}^{-T/2} \otimes \mathbf{R}^{-1/2} \right) \left[\begin{array}{c} \frac{\partial \mathbf{h}}{\partial \boldsymbol{\varphi}^T} \mid \frac{\partial \mathbf{h}}{\partial \boldsymbol{\rho}^T} \mid \frac{\partial \mathbf{h}}{\partial \sigma_n^2} \end{array} \right] \\ &= [\mathbf{U}_\psi \mid \mathbf{V}_s \mid \mathbf{V}_n]. \end{aligned} \quad (72)$$

The k th column of \mathbf{U}_θ , $\mathbf{U}_{\sigma_\theta}$, \mathbf{U}_ψ , \mathbf{V}_s and \mathbf{V}_n is given by

$$\mathbf{U}_\theta(:, k) = \text{vec} \left\{ \mathbf{R}^{-1/2} \frac{\partial \mathbf{R}}{\partial \theta_k} \mathbf{R}^{-1/2} \right\} \quad (73)$$

$$\mathbf{U}_\beta(:, k) = \text{vec} \left\{ \mathbf{R}^{-1/2} \frac{\partial \mathbf{R}}{\partial \beta_k} \mathbf{R}^{-1/2} \right\} \quad (74)$$

$$\mathbf{U}_{\sigma_\theta}(:, k) = \text{vec} \left\{ \mathbf{R}^{-1/2} \frac{\partial \mathbf{R}}{\partial \sigma_{\theta k}} \mathbf{R}^{-1/2} \right\} \quad (75)$$

$$\mathbf{U}_{\sigma_\beta}(:, k) = \text{vec} \left\{ \mathbf{R}^{-1/2} \frac{\partial \mathbf{R}}{\partial \sigma_{\beta k}} \mathbf{R}^{-1/2} \right\} \quad (76)$$

$$\mathbf{U}_\psi(:, k) = \text{vec} \left\{ \mathbf{R}^{-1/2} \frac{\partial \mathbf{R}}{\partial \varphi} \mathbf{R}^{-1/2} \right\} \quad (77)$$

$$\mathbf{V}_s(:, k) = \text{vec} \left\{ \mathbf{R}^{-1/2} \frac{\partial \mathbf{R}}{\partial \rho_k} \mathbf{R}^{-1/2} \right\} \quad (78)$$

$$\mathbf{V}_n(:, k) = \text{vec} \left\{ \mathbf{R}^{-1/2} \frac{\partial \mathbf{R}}{\partial \sigma_n^2} \mathbf{R}^{-1/2} \right\}. \quad (79)$$

Then we can rewrite (69) as

$$\frac{2}{T} \mathbf{F} = \begin{bmatrix} \mathbf{U}^H \\ \mathbf{V}^H \end{bmatrix} [\mathbf{U} \quad \mathbf{V}]. \quad (80)$$

By taking the upper-left corner of \mathbf{F}^{-1} and resorting to the block matrix inversion lemma [32], we can derive the interested angle parameters $CRB(\boldsymbol{\eta})$ from (67).

Remark 1: The major computational effort of the proposed algorithm includes the construction of $\hat{\mathbf{R}}$, performing EVD on $\hat{\mathbf{R}}$, spectral searching and Step 6. Denote the number of searches for estimating the center DOAs $\hat{\theta}$ and $\hat{\beta}$ by Δ_θ and Δ_β , respectively. To calculate $\hat{\mathbf{R}}$ and perform EVD on $\hat{\mathbf{R}}$, a computational complexity of $O((2F)^2T)$ and $O((2F)^3)$ is needed, respectively. The complexity for two 1D spectral searches in Step 4 is about $O(\Delta_\theta(8M_1K^2 + 16M_1^2K) + \Delta_\beta(8N_1K^2 + 16N_1^2K))$. The complexity of Step 6 is $O(8FK^2 + 2(2F)^2K)$. The total computational complexity of the proposed algorithm is about $O((2F)^2T + (2F)^3 + \Delta_\theta(8M_1K^2 + 16M_1^2K) + \Delta_\beta(8N_1K^2 + 16N_1^2K) + 8FK^2 + 2(2F)^2K)$. Because Cao's algorithm does not make use of noncircularity characteristics of the signal, the dimension of the covariance matrix is $F \times F$, and its required

computational complexity is about half of the proposed algorithm, as shown in Table III.

Remark 2: Here, the maximum number of distinguishable signals of the proposed algorithm is analyzed as compared to Cao's algorithm [18]. With the additional information provided by noncircular signals, the maximum number of signals distinguished by the proposed algorithm is based on the new extended data vector in (21) as well as the matrix $\mathbf{D}(\theta)$ in (44) and the matrix $\mathbf{D}(\beta)$ in (50), which is shown in Table III as compared to Cao's algorithm. Obviously, the proposed algorithm can distinguish twice the number of signals than that of Cao's algorithm.

V. SIMULATION RESULTS

In this part, simulations are provided to demonstrate the effectiveness of the proposed estimator for ID noncircular sources in comparison with Cao's algorithm [18]. The CRB for 2D angular parameter estimation of ID noncircular sources is also plotted as a benchmark. In all simulations, an L-shaped array with $F = M + N - 1 = 13$ ($M = N = 7$) sensors is considered, with multiple BPSK signals impinging. The variance of ray-gains is set as $\{\sigma_{\gamma_k}^2\}_{k=1}^K = 1$, and the number of scattering paths is set as $\{L_k\}_{k=1}^K = 100$. We use the root mean square

error (RMSE) $RMSE(\theta) = \sqrt{\frac{1}{KM_c} \sum_{k=1}^K \sum_{m=1}^{M_c} (\hat{\theta}_{k,m} - \theta_k)^2}$

and $RMSE(\beta) = \sqrt{\frac{1}{KM_c} \sum_{k=1}^K \sum_{m=1}^{M_c} (\hat{\beta}_{k,m} - \beta_k)^2}$ as the performance index, where M_c is the total number of Monte-Carlo trials, $\hat{\theta}_{k,m}$ and $\hat{\beta}_{k,m}$ are the estimate of the 2D center DOAs θ_k and β_k of the k th signal in the m th Monte-Carlo trial, respectively. The number of sensors in each subarray is $M_1 = N_1 = 6$ for the proposed algorithm.

In the first simulation, shown in Fig. 2, we examine the scatter plot of 2D center DOAs θ and β estimated by the proposed algorithm. Here, we consider four ID noncircular signals with angular parameters $(\theta_1, \sigma_{\theta_1}, \beta_1, \sigma_{\beta_1}) = (50^\circ, 0.5^\circ, 85^\circ, 0.5^\circ)$, $(\theta_2, \sigma_{\theta_2}, \beta_2, \sigma_{\beta_2}) = (75^\circ, 0.5^\circ, 60^\circ, 0.5^\circ)$, $(\theta_3, \sigma_{\theta_3}, \beta_3, \sigma_{\beta_3}) = (90^\circ, 0.5^\circ, 70^\circ, 0.5^\circ)$, and $(\theta_4, \sigma_{\theta_4}, \beta_4, \sigma_{\beta_4}) = (65^\circ, 0.5^\circ, 95^\circ, 0.5^\circ)$. All signals' angular distributions are Gaussian with the same angular spread. The SNR is set as 20dB, and the number of the snapshots is $T = 1000$. According to Remark 2, the maximum number of 2D ID noncircular signals that can be handled by Cao's algorithm is 3, while for the proposed one it is 6. Fig. 2 displays

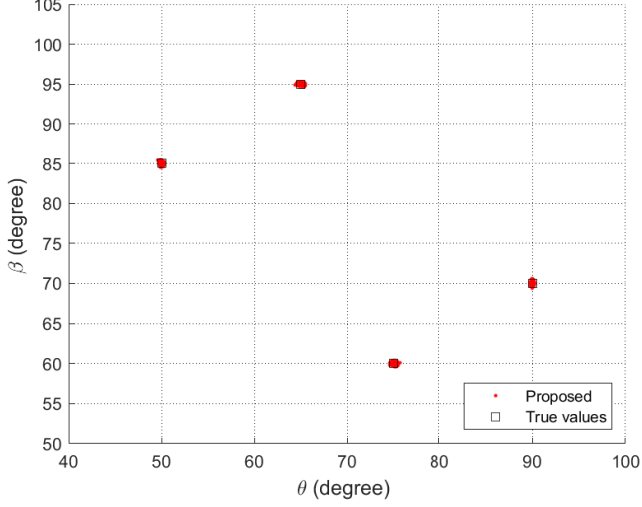


Fig. 2: 2D center DOA scatter plot for ID noncircular sources.

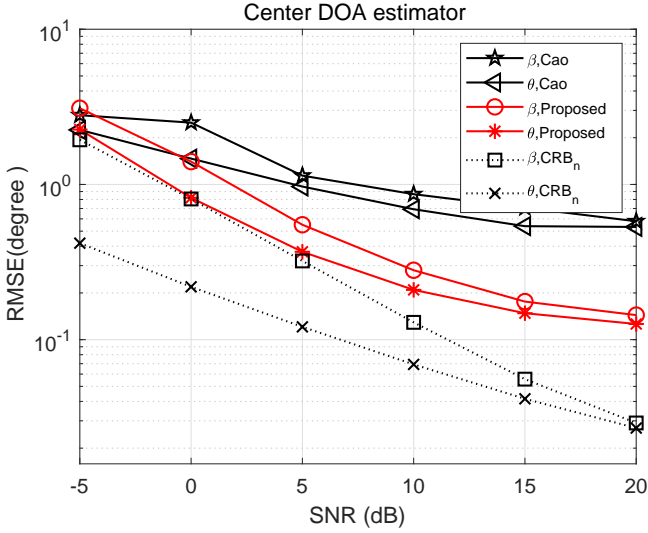


Fig. 3: RMSE of 2D center DOAs for ID noncircular sources versus SNR.

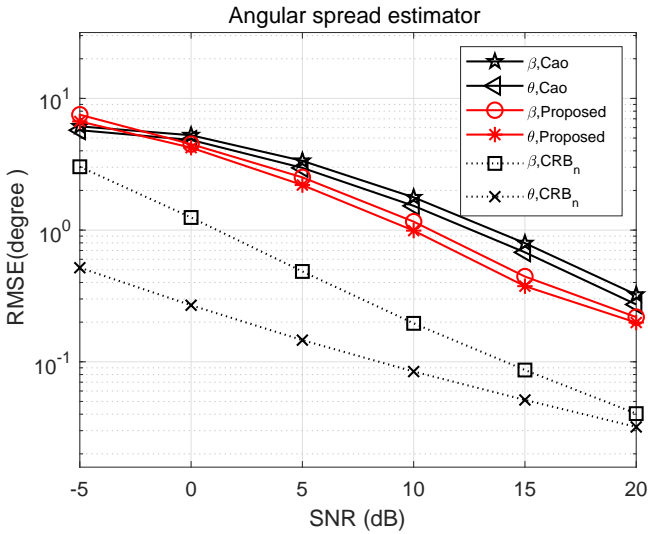


Fig. 4: RMSE of 2D angular spreads for ID noncircular sources versus SNR.

the 2D DOA scattergram of the ID noncircular signals by the proposed algorithm. It can be seen that the proposed algorithm has provided an effective estimation result.

In the second simulation, the performance of the proposed algorithm is studied with SNR varying from -5dB to 20dB. There are two uncorrelated ID noncircular signals with angular parameters $(\theta_1, \sigma_{\theta_1}, \beta_1, \sigma_{\beta_1}) = (40^\circ, 0.5^\circ, 30^\circ, 0.5^\circ)$, and $(\theta_2, \sigma_{\theta_2}, \beta_2, \sigma_{\beta_2}) = (60^\circ, 0.5^\circ, 50^\circ, 0.5^\circ)$. Their angular distribution is Gaussian with the same angular spread. The number of snapshots is 300 and $M_c = 200$. When the number of array sensors on the x-axis is 7, the proposed algorithm divides the array on the x-axis into two 6-sensor subarrays and two 6-sensor extended subarrays. The processing at z-axis is the same as the array on the x-axis. However, Cao's algorithm only divides the array on the x-axis or the z-axis into two subarrays with 6 sensors. Fig. 3 and Fig. 4 illustrate the RMSEs of the 2D center DOA estimation and the 2D angular spread estimation for different algorithms, respectively. The CRBs are also shown as benchmarks. It can be observed that, with the additional noncircularity information exploited, the performance of the proposed algorithm is better than Cao's algorithm.

In the third simulation, the performance with respect to a varying number of snapshots ranging from 50 to 950 is investigated. The SNR is set at 15dB and the other parameters are the same as in the second simulation. As shown in Fig. 5 and Fig. 6, a similar conclusion can be drawn as in Fig. 3 and Fig. 4, i.e., as the number of snapshots increases, the proposed algorithm again outperformed Cao's algorithm [18], and both performances improve gradually.

In the fourth simulation, the performance of the proposed algorithm is studied versus the angular spread varying from 0.2° to 3.4° . The SNR is set at 10dB, the angular spread of two uncorrelated ID noncircular signals is set as the same, and the other parameters are the same as in the second simulation. From Fig. 7, it can be seen that as the angular spread increases, the estimation performance of the 2D center DOA of both algorithms becomes worse overall. It can also be observed from Fig. 8 that the RMSE of the proposed method reaches a minimum when the angular spread is at an intermediate value. When the angular spreads are small, noise is the main influencing factor and it is expected that the performance will become better. When the angular spreads are large, the rest of Taylor series in (7) cannot be omitted. As a result, their RMSE will increase. However, with the increase of the angular spread, the proposed algorithm still shows better performance than Cao's algorithm [18] in both 2D center DOA estimation and 2D angular spread estimation.

In the last simulation, we consider the case where multiple ID noncircular signals have different angular distributions. Two ID noncircular signals are considered, one with 2D center DOAs $(\theta_1, \beta_1) = (40^\circ, 30^\circ)$ and exhibiting Gaussian distribution with $(\sigma_{\theta_1}, \sigma_{\beta_1}) = (0.5^\circ, 0.5^\circ)$, another with center DOAs $(\theta_2, \beta_2) = (60^\circ, 50^\circ)$ and exhibiting uniform distribution with $(\sigma_{\theta_2}, \sigma_{\beta_2}) = (0.5^\circ, 0.5^\circ)$. The RMSE results for different algorithms are shown in Figs. 9 and 10. It is indicated that the proposed algorithm can also work effectively when multiple ID noncircular signals have different angular distributions. In

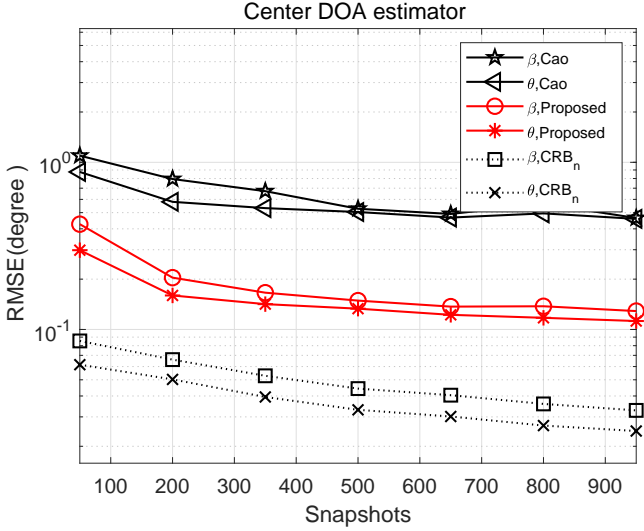


Fig. 5: RMSE of 2D center DOAs for ID noncircular sources versus number of snapshots.

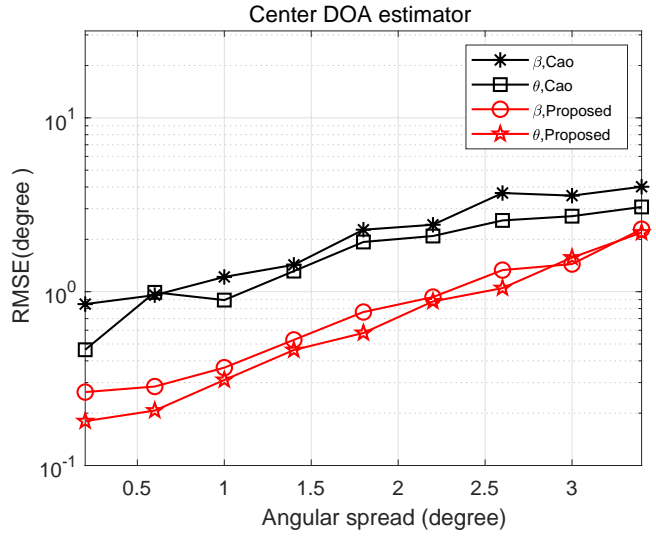


Fig. 7: RMSE of 2D center DOAs for ID noncircular sources versus the angular spread.

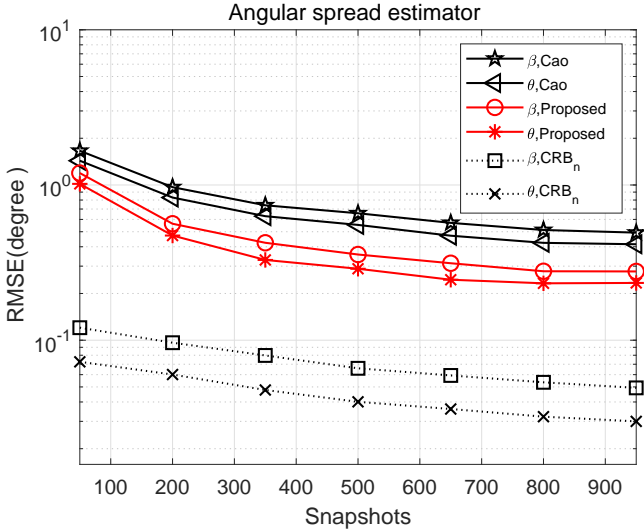


Fig. 6: RMSE of 2D angular spreads for ID noncircular sources versus number of snapshots.

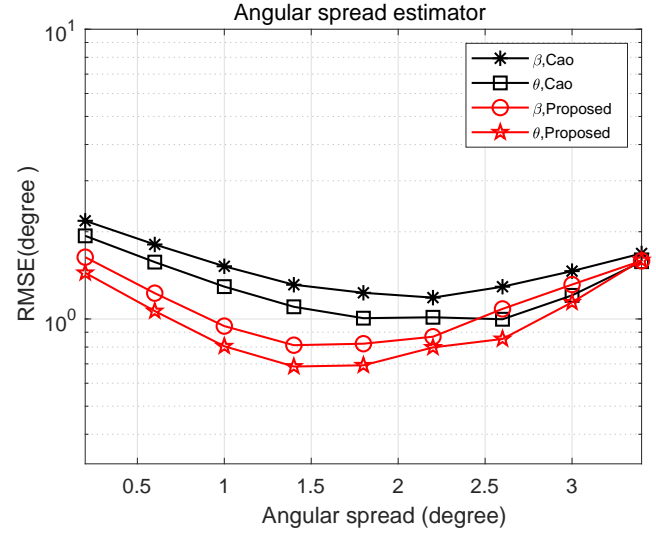


Fig. 8: RMSE of 2D angular spreads for ID noncircular sources versus the angular spread.

addition, for each type of angular distribution, the proposed algorithm has achieved a more accurate result than Cao's algorithm [18].

VI. CONCLUSION

In this paper, a novel angular parameter estimation algorithm for multiple 2D incoherently distributed noncircular sources has been developed based on the reduced-rank principle. By utilizing the noncircularity property of signals, an extended GAM model for the L-shaped array structure is derived with Taylor series expansion, and the two center DOA angles associated with each source are estimated separately through spectral peak search exploiting the noncircularity-based generalized rotational invariance relationship. The pairing of the two center DOAs is completed by searching for the minimum value of the cost function. Finally, closed-form solutions for 2D angle spreads are calculated by the central moments of the angular distribution. Moreover, the CRB for the concerned

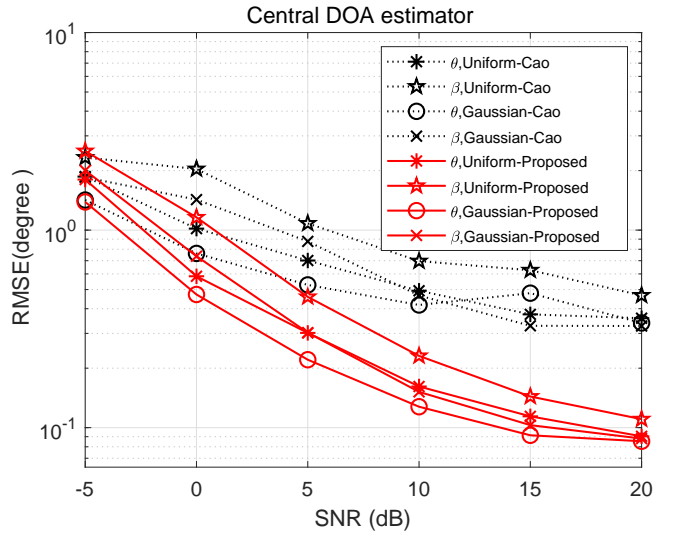


Fig. 9: RMSE of 2D center DOAs with different distributed angular distributions.

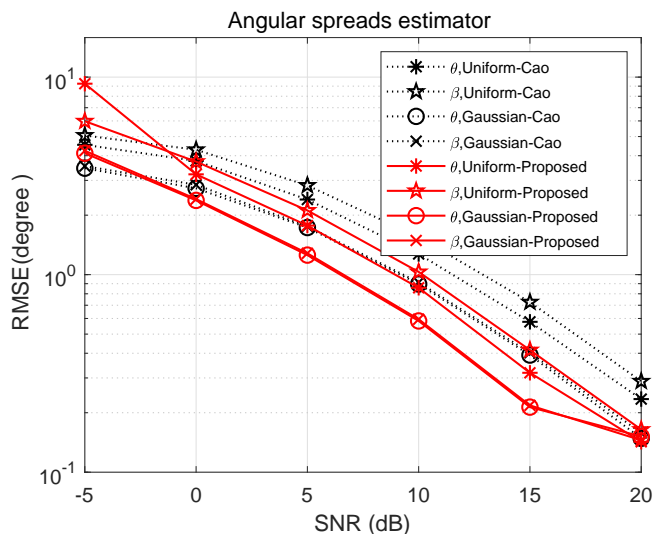


Fig. 10: RMSE of 2D angular spreads with different distributed angular distributions.

problem is derived as a benchmark. The superiority of the proposed algorithm has been demonstrated by various simulation results.

REFERENCES

- [1] F. F. Gao, Z. Tian, E. G. Larsson, M. Pesavento and S. Jin, "Introduction to the special issue on array signal processing for angular models in Massive MIMO communications," *IEEE J. Sel. Topics Signal Process.*, vol. 13, no.5, pp. 882-885, Sept. 2019.
- [2] F. Wen, J. Shi and Z. Zhang, "Joint 2D-DOD, 2D-DOA and polarization angles estimation for bistatic EMVS-MIMO radar via PARAFAC analysis," *IEEE Trans. Veh. Technol.*, vol. 69, no. 2, pp. 1626-1638, Feb. 2020.
- [3] X. Wang, L. Wan, M. Huang, C. Shen, Z. Han and T. Zhu, "Low-complexity channel estimation for circular and noncircular signals in virtual MIMO vehicle communication systems," *IEEE Trans. Veh. Technol.*, vol. 69, no. 4, pp. 3916-3928, Apr. 2020.
- [4] Z. Zheng, W. Wang, Y. Kong, and Y. D. Zhang, "MISC array: A new sparse array design achieving increased degrees of freedom and reduced mutual coupling effect," *IEEE Trans. Signal Process.*, vol. 67, no. 7, pp. 1728-1741, Apr. 2019.
- [5] H. Chen, W. F. Wang and W. Liu, "Joint DOA, range, and polarization estimation for rectilinear sources with a COLD array," *IEEE Wirel. Commun. Lett.*, vol. 8, no. 5, pp. 1398-1401, Oct. 2019.
- [6] F.-G. Yan, X. Li, C. Chen, M. Jin., "Sector unitary MUSIC," *Signal Process.*, vol. 168, Art. no. 107341, Mar. 2020.
- [7] J. Shi, G. Hu, X. Zhang, F. Sun, and H. Zhou, "Sparsity-based two-dimensional DOA estimation for coprime array: From sum-difference coarray viewpoint," *IEEE Trans. Signal Process.*, vol. 65, no. 21, pp. 5591-5604, Nov. 2017.
- [8] S. Valaee, B. Champagne, and P. Kabal, "Parametric localization of distributed sources," *IEEE Trans. Signal Process.*, vol. 43, no. 9, pp. 2144-2153, Sept. 1995.
- [9] S. Shahbazpanahi, S. Valaee, and M. Bastani, "Distributed source localization using esprit algorithm," *IEEE Trans. Signal Process.*, vol. 49, no. 10, pp. 2169-2178, Oct. 2001.
- [10] A. Zoubir and Y. Wang, "Efficient DSPE algorithm for estimating the angular parameters of coherently distributed sources," *Signal Process.*, vol. 88, no. 4, pp. 1071-1078, Apr. 2008.
- [11] W.Y. Chen, X.F. Zhang, L. Xu and Q.L. Cheng, "Successive DSPE-based coherently distributed sources parameters estimation for unmanned aerial vehicle equipped with antennas array," *Phys. Commun.*, vol. 32, pp. 96-103, 2019.
- [12] Y. Tian, H. Yue and X. Rong, "Multi-parameters estimation of coherently distributed sources under coexistence of circular and noncircular signals," *IEEE Commun. Lett.*, vol. 24, no. 6, pp. 1254-1257, Jun. 2020.
- [13] W.M. Xiong, J. Picheral, S. Marcos, "Performance analysis of distributed source parameter estimator (DSPE) in the presence of modeling errors due to the spatial distributions of sources," *Signal Process.*, vol. 143, pp. 146-151, Feb. 2018.
- [14] J.A. Chaaya, J. Picheral and S. Marcos, "Localization of spatially distributed near-field sources with unknown angular spread shape," *Signal Process.*, vol. 106, pp. 259-265, Jan. 2015.
- [15] Y. Meng, P. Stoica and K. Wong, "Estimation of the directions of arrival of spatially dispersed signals in array processing," *Proc. IEE Radar, Sonar, Navig.*, vol. 143, no. 1, pp. 1-9, Feb. 1996.
- [16] O. Besson and P. Stoica, "Computationally efficient maximum likelihood approach to DOA estimation of a scattered source," *Wireless Pers. Commun.*, vol. 16, no. 2, pp. 135-148, 2001.
- [17] S. Shahbazpanahi, S. Valaee and A. B. Gershman, "A covariance fitting approach to parametric localization of multiple incoherently distributed sources," *IEEE Trans. Signal Process.*, vol. 52, no. 3, pp. 592-600, Mar. 2004.
- [18] R. Z. Cao, F. F. Gao and X. F. Zhang, "An angular parameter estimation method for incoherently distributed sources via generalized shift invariance," *IEEE Trans. Signal Process.*, vol. 64, no. 17, pp. 4493-4503, Sept. 2016.
- [19] Z. Zheng, J. Lu, W. Q. Wang, H. F. Yang and S. S. Zhang, "An efficient method for angular parameter estimation of incoherently distributed sources via beamspace shift invariance," *Digital Signal Process.*, vol.83, pp. 261-270, 2018.
- [20] J. Zhuang, H. Xiong, W. Wang and Z. Chen, "Application of Manifold Separation to Parametric Localization for Incoherently Distributed Sources," *IEEE Trans. Signal Process.*, vol. 66, no. 11, pp. 2849-2860, Jun. 2018.
- [21] J. Zhou, Z. Zheng and G. J. Li, "Low-complexity estimation of the nominal azimuth and elevation for incoherently distributed sources," *Wireless Pers. Commun.*, vol. 71, no. 3, pp. 1777-1793, 2013.
- [22] A. Hu, T. Lv, H. Gao, Z. Zhang and S. Yang, "An ESPRIT-based approach for 2-D localization of incoherently distributed sources in massive MIMO systems," *IEEE J. Sel. Topics Signal Process.*, vol. 8, no. 5, pp. 996-1011, Oct. 2014.
- [23] T. Lv, F. Tan, H. Gao and S. Yang, "A beamspace approach for 2-D localization of incoherently distributed sources in massive MIMO systems," *Signal Process.*, vol. 121, pp. 30-45, 2016.
- [24] Z. Zheng, W. Wang, H. Meng, H. Cheung and H. Zhang, "Efficient beamspace-based algorithm for 2-D DOA estimation of incoherently distributed sources in massive MIMO systems," *IEEE Trans. Veh. Technol.*, vol. 67, no. 12, pp. 11776-11789, Dec. 2018.
- [25] Y. L. Huang, Y. G. Xu, Y. Lu and Z. W. Liu, "Aligned propagator scanning approach to DOA estimation of circular and noncircular wideband source signals," *IEEE Trans. Veh. Technol.*, vol. 68, no. 2, pp. 1702-1717, Feb. 2019.
- [26] P. Gupta and M. Agrawal, "Design and analysis of the sparse array for DOA estimation of noncircular signals," *IEEE Trans. Signal Process.*, vol. 67, no. 2, pp. 460-473, Jan. 2019.
- [27] H. Chen, C. P. Hou, W. P. Zhu, W. Liu, Y. Y. Dong, Z. J. Peng and Q. Wang, "ESPRIT-like two-dimensional direction finding for mixed circular and strictly noncircular sources based on joint diagonalization," *Signal Process.*, vol. 141, pp. 48-56, Dec. 2017.
- [28] X. Wang, L. Wan, M. Huang, C. Shen and K. Zhang, "Polarization channel estimation for circular and non-circular signals in massive MIMO systems," *IEEE J. Sel. Topics Signal Process.*, vol. 13, no. 5, pp. 1001-1016, Sept. 2019.
- [29] S. B. Hassen, F. Bellili, A. Samet and S. Affes, "Angular parameters estimation of multiple incoherently distributed sources generating non-circular signals," *IEEE Access.*, vol. 7, pp. 38451-38468, 2019.
- [30] X. M. Yang, G. J. Li, C. C. Ko, Z. Zheng and T. S. Yeo, "Central DOA estimation of incoherently distributed noncircular sources with cross-correlation matrix," *Circuits Syst. Signal Process.*, vol. 34, pp. 3697-3707, 2015.
- [31] X. Yang, Z. Zheng and B. Hu, "Off-grid DOA estimation of incoherently distributed non-circular sources via generalised approximate message passing," *Electron. Lett.*, vol. 52, no. 4, pp. 262-264, Jan. 2016.
- [32] Z. L. Dai, B. Ba, W. J. Cui and Y. M. Sun, "Computational efficient two-dimension DOA estimation for incoherently distributed noncircular sources with automatic pairing," *IEEE Access.*, *IEEE Access.*, vol. 5, pp. 20249-20259, 2017.
- [33] Z. Huang, X. Li, P. Huang, and W. Wang, "DOA estimation for incoherently distributed sources considering mixed circular and noncircular signals in massive MIMO system," *IEEE Access.*, vol. 7, pp. 106900-106911, 2019.

- [34] H. Abeida and J. P. Delmas, "Direct derivation of the stochastic CRB of DOA estimation for rectilinear sources," *IEEE Signal Process. Lett.*, vol. 24, no. 10, pp. 1522-1526, Oct. 2017.